DPR-CAE: Capsule Autoencoder with Dynamic Part Representation for Image Parsing

Canqun Xiang, Zhennan Wang, Wenbin Zou, Chen Xu
Shenzhen University
{xiangcanqun2018, wangzhennan2017, wzou, xuchen_szu}@email.szu.edu.cn

Abstract

Parsing an image into a hierarchy of objects, parts, and relations is important and also challenging in many computer vision tasks. This paper proposes a simple and effective capsule autoencoder to address this issue, called DPR-CAE. In our approach, the encoder parses the input into a set of part capsules, including pose, intensity, and dynamic vector. The decoder introduces a novel dynamic part representation (DPR) by combining the dynamic vector and a shared template bank. These part representations are then regulated by corresponding capsules to composite the final output in an interpretable way. Besides, an extra translation-invariant module is proposed to avoid directly learning the uncertain scene-part relationship in our DPR-CAE, which makes the resulting method achieves a promising performance gain on rm-MNIST and rm-Fashion-MNIST. DPR-CAE can be easily combined with the existing stacked capsule autoencoder and experimental results show it significantly improves performance in terms of unsupervised object classification. Our code is available in the Appendix.

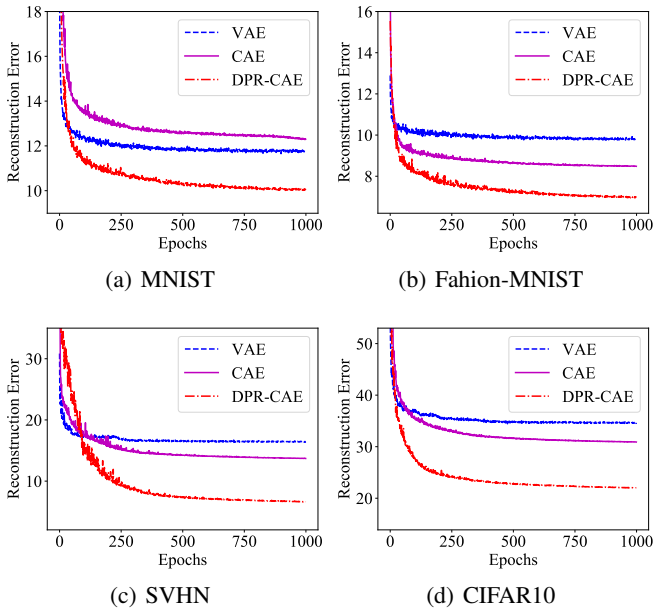

(a) MNIST (b) Fahion-MNIST

(c) SVHN (d) CIFAR10

Figure 1: Reconstruction error on val datasets. CAE implies capsule autoencoder. DPR-CAE outperforms its counterparts on all datasets.

1 Introduction

Capsule networks [Hinton *et al.*, 2011; Sabour *et al.*, 2017] are designed to understand images, which parse an image into a hierarchy of objects, parts and relations. Studies show that infants form early object perception by dividing visual inputs into simple part units in an unsupervised way. Inspired by this and recent works on parts discovery, we propose an unsupervised capsule-based method for learning visual part representation.

Most of the existing capsule networks [Sabour *et al.*, 2017; Hinton *et al.*, 2018] represent a part by a vector or matrix. Which brings some drawbacks that limit its development: 1) These forms of part representation are the latent state of part units, thus lacking of flexibility and intuition. 2) Adjacent capsules repeatedly represent many part units due to the shared receptive field, which is redundant and inefficient. Stacked capsule network [Kosiorek *et al.*, 2019] and [Tieleman, 2014] propose a novel part representation approach, in which the object is encoded by capsules and corresponding static templates as few as possible. These approaches can find various meaningful parts that can be directly observed in grayscale/color space. However, the capability of every part representation is restricted by the corresponding static template that is fixed in the inference phase. Besides, all these methods above focus on encoding object-part relationships. It is making them difficult to handle the case where the relative coordinate between scene and object is changed. For instance, when a human's vision system parses the parts and object-part relationships in a nature scene, the first step is to locate the object in the scene and then to find the parts from the object. Though capsule networks are effective in learning the relationships between object and parts, they fail to learn the uncertain scene-part relationship directly.

To tackle the above problems, we propose a novel capsule network, called DPR-CAE. Our method is developed based on the autoencoder framework and trained in an unsupervised way. The encoder parses the input into a set of part capsules,

which include pose, intensity, and dynamic vector. The decoder first generates a set of dynamic part representations by combining the dynamic vector and template bank that is a group of trainable parameter matrices and is shared by all part capsules. These part representations are then regulated by corresponding capsules to composite the final output. Dynamic part representation introduces a set of rich and various forms to explain the part units, which enhances the overall capability of our model to represent a complex object. As shown in Figure 3, each step of our decoder is highly interpretable. Motivated by the human visual working mechanism, we further propose a translation-invariant module to avoid directly learning uncertain scene-part relationships in our model. The translation-invariant module maps the object discovered from the scene into a standard coordinate frame, ensuring that the input is translation invariant. This strategy is critically important for our model to focus on encoding object-part relationships. After obtaining the synthesized object, the translation-invariant module easily restores the object to the scene through the inverse transformation. Our method achieves superior performance over its counterparts, as reported in Figure 1. The main contributions of this paper are summarized as follows:

- We propose a simple and effective capsule network framework, called DPR-CAE, which is of high interpretability by visualizing its decoding procedure.
- We introduce a dynamic part representation method to generate rich and various part representations, which endows our model with powerful capability for representing complex inputs.
- A translation-invariant module is proposed to avoid directly learning the uncertain scene-part relationships in our model, which enhances the model's robustness.
- We extend the DPR-CAE into the stacked capsule autoencoder, namely DPR-SCAE, which obtains state-of-the-art performance in unsupervised classification.

2 Related Works

Recently, capsule networks have achieved impressive performance in various tasks. Capsule networks are designed to parse an image into a hierarchy of objects, parts and relations. [Hinton *et al.*, 2011] first introduced the idea of capsule networks. [Sabour *et al.*, 2017] revisited the capsule concept and introduced capsule framework for image classification [Zhang *et al.*, 2018]. Subsequent works are produced to improve the routing algorithms [Hinton *et al.*, 2018; Taeyoung *et al.*, 2019] and scale to other tasks [Duarte *et al.*, 2019; Xiang *et al.*, 2020; Edraki *et al.*, 2020].

Part representation has been explored by [Kosiorek *et al.*, 2019]. Such a method relies on an autoencoder framework to find meaningful part units and part-whole relationships, which achieves state-of-the-art performance in unsupervised object classification. [Tieleman, 2014] parses an image into part capsules, then recovers the image by these capsules with specific-domain knowledge. However, both above methods directly use a static template for per part capsule as the part representation, which limits its overall representation when challenging a complex dataset. We propose a dynamic part representation fashion for part capsules to obtain rich and various representations.

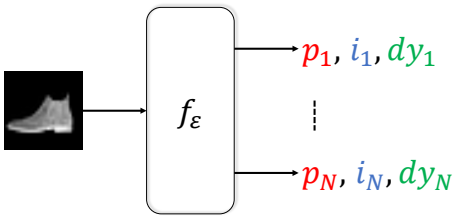

Figure 2: Part encoder. The encoder f_ε parses an image into a set of part capsules, each comprising a pose vector p_n, a scalar intensity value i_n, and a dynamic vector dy_n.

The object-part relationships are encoded by a routing mechanism in most of existing capsule networks [Ribeiro *et al.*, 2020b; Ribeiro *et al.*, 2020a]. An iterative routing-by-agreement mechanism is used in [Sabour *et al.*, 2017] and its improved versions [Xiang *et al.*, 2018; Wang and Liu, 2018]. In such methods, a lower-level capsule prefers to sent its output to higher level capsules whose activity vectors have a big scalar product with the prediction coming from the lower-level capsule. [Hinton *et al.*, 2018] represents object-part relationships by trainable viewpoint-invariant transformation matrices, which are trained discriminatively by backpropagating through the unrolled iterations of EM between each pair of adjacent capsule layers. However, these relationships usually remain untouched and only work well in a standard coordinate system. In our method, we first introduce an extra translation-invariant module to build the relationship between scene and object and then focus on the relationship between object and part by the capsule autoencoder. This step-by-step manner endows our model with more robustness.

3 Capsule Autoencoder

In this section, we describe a method to understand an image, called *DPR-CAE*. We build our framework upon classical encoder-decoder manner with specific-domain knowledge. The encoder segments image into parts (object→parts), and the decoder then learns to model sets parts as arrangements of an object (parts→object), which are visually explainable. Further, to map the object from the scene into a canonical coordinate frame (scene→object), we introduce a translation-invariant module, which dramatically enhances the robustness of our model. In what follows we describe the form of the proposed part encoder and object decoder in first two subsections. Then, the subsequent section describes the translation-invariant module and training procedure.

3.1 Part Encoder

Explaining images as geometrical arrangements of parts requires 1) discovering what parts are there in an image and 2) inferring the relationships of the parts to their pose. Hence, the purpose of part encoder is to find the latent attributes of part capsules and to explore the part-whole relationship. The part encoder framework is shown in Figure 2, which is a structural neural network f_ε. Its input is the raw image

$y \in [0,1]^{h \times w \times c}$, and its output attempts to encode a vector graphics description of that image, the attributes of parts and relationship are encoded by these vectors. We formulate part encoder as follows:

$$p_{1:N}, i_{1:N}, dy_{1:N} = f_\varepsilon(y) \tag{1}$$

where p_n, i_n, dy_n are deemed as the description of part capsule n. p ($\in \mathbb{R}^6$) indicates the poses of part capsules, which is an affine transformation matrix. i ($\in \mathbb{R}$) implies the relative intensity of per part capsule. If a part capsule exists, the corresponding intensity will be large. dy ($\in \mathbb{R}^A$) is the dynamic coefficients, which is critical for the proposed dynamic part representation. f_ε is a CNN followed by a bottom-up attention mechanism based on global-average pooling (details in Appendix.A). In the part encoder, we limit the maximum number of part capsules to N.

3.2 Object Decoder

Object decoder architecture is engineered using domain-specific knowledge. It is designed to decode codes in a specific type of vector graphics description. As shown in Figure 3, we formulate the object decoder as follows:

$$\hat{T}_{1:N} = Relu6((dy_{1:N} * T) \cdot 6)/6 \tag{2}$$

$$\hat{O}_{1:N} = TransformImage(\hat{T}_{1:N}, p_{1:N}) \tag{3}$$

$$O = log(\sum^{N} exp(i_{i:N} \cdot \hat{O}_{1:N} \cdot C))/C \tag{4}$$

where $*$ is a convolution operation, T is a set of learned templates, $Relu6(\cdot)$ is a modification of the rectified linear unit where we limit the activation to a maximum size of 6. Equation (2) is the key step to obtain dynamic part representation, which endows the model a powerful expressiveness. $TransformImage(\cdot)$ is an affine-transform operation that transform the dynamic part template $\hat{T}_n$ into the model output according to the pose p_n. Equation (4) combines the contributions from all part capsules, where C is a constant. We discuss each part in detail in the next few subsections.

Template bank

The decoder first initializes an image template bank T similar to [Tieleman, 2014; Kosiorek *et al.*, 2019], the number of template T is same as the dimensional of dy encoded by the part encoder. Template $T_a \in [0,1]^{h_t \times w_t \times c}$ is smaller than the image y. In the decoder, the capsule essentially copies the template into the model output, at the location and intensity that are specified in the two code vectors a.k.a p, i. After the model is trained, Template T becomes a constant, so the expressive ability of the model is severely limited by the final form of T.

Dynamic part representation

Different from previous works [Tieleman, 2014; Kosiorek *et al.*, 2019], the template bank T is shared by all part capsules rather than limited to taking a fixed template per capsule in our method. We obtain a dynamic part template for per capsule by Equation (2). For each part capsule, a group of dynamic coefficients dy is encoded by the part encoder, which learns to combine the template bank T and achieves a new part template/representation $\hat{T}$ for corresponding part capsule. The dynamic coefficients dy are scaled into $[-1,1]$ by activation function $tanh(\cdot)$ in practice. Dynamic template $\hat{T}$ provides differentiated representation for every data case, which greatly enhances the model's expressive ability.

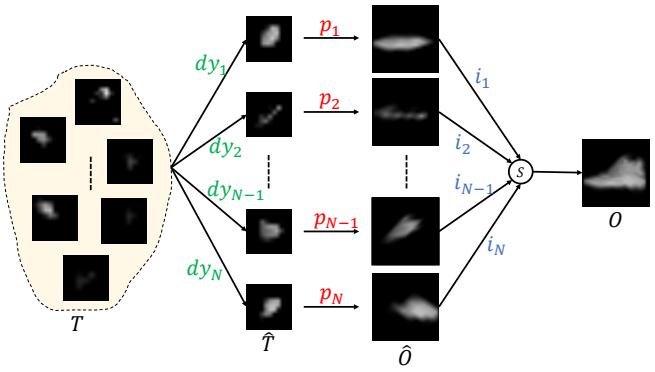

Figure 3: Object decoder. The part representations of an image are dynamically generated by combining template bank T with a dynamic vector dy_n. Part representations are then transformed into image coordinates, using p_n, and summed according to the relative intensity i_n, yielding a composited object.

Part-object representation

The part-object representations $\hat{O}$ reflect the relationships between parts and a whole object. The part representations are transformed from the part natural coordinate frame into a natural coordinate frame of a whole object by an approximative affine-transformation matrix p. It is tempting to exploit other effects of viewpoint changes by replicating parts across scale, orientation, and other affine degrees of freedom. Here, we follow [Jaderberg *et al.*, 2015] to implement the affine transformation.

Composite object

The final step of object decoder is to compose object O from these part-object representations $\hat{O}$. For each pixel in object O, there are N pixel contributions from corresponding positions of part-object representations $\hat{O}$. The most intuitive way is to simply add them up. However, when we're deciding what the value of a particular output pixel should be, we want to use the largest of the capsules' contributions instead of the sum. On the one hand, linear summation easily causes the model to lose expression diversity due to all part capsules participate in the reconstruction process without a difference. On the other hand, if we select the greatest one as the output, the learning signal disappears for all capsules apart from the one with the greatest output to a particular pixel. Thus, we adopt a more sophisticated way, as shown in Equation (4), which is a nonlinear function and works better in our experiments. Here, C is a hyperparameter, and we set it to 70 in experiments. This function is a softened version of the max function and strengthens the differentiability among pixels from the same spatial position while ensuring that all part capsules participate in learning.

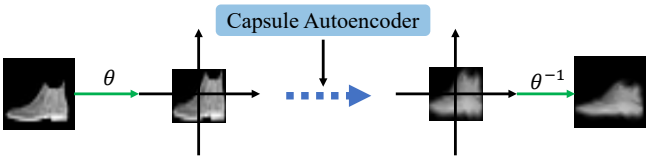

Figure 4: Translation-invariant module. θ is a four-dimensional pose (two translations, two scales), which locates the object and scales to a standard coordinate frame. θ^{-1} is inverse of θ.

3.3 Translation-Invariant Module

The pose p encodes the relative transformation between part and object (object→part) rather than between part and scene (scene→part), so it is sensitive to the varying position of an object in the scene (scene→object). As shown in Figure 4, an intuitive way to solve this problem is to encode the relative position θ (object pose) of a whole object in the scene before part encoder, and then recover it by the inverse matrix θ^{-1} after the object decoder. θ is a four-dimensional vector (two scales, two translations), which is learned by a simple neural network (details in Appendix.B). The input of the capsule autoencoder is translation invariant after transforming the object into a standard coordinate frame by the parameter θ. Thus, the capsule autoencoder only needs to focus on encoding the relative relationship between part and object, which is beneficial for exploring the latent architecture of the object. This module can be naturally embedded in our method without additional supervision information.

3.4 Training

The purpose of the capsule autoencoder is to reconstruct the input y by the encoded part capsules and a shared template bank. We define the objective function as $L_{reg} = 1/2 \times (y - O)^2$ to cause the distance between composite object O and input y as close as possible. Some efficient sparsity strategies are adopted to achieve sparse and diverse capsule representations. We define the sparsity terms as follows:

$$L_{s1} = \frac{1}{B}\sum_{1}^{B}(\sum_{1}^{N} I_n - K)^2 \tag{5}$$

$$L_{s2} = \frac{1}{N}\sum_{1}^{N}(\sum_{1}^{B} I_b - \frac{B \times K}{N})^2 \tag{6}$$

where K ($\in [1, ..., N]$) is a constant. I ($\in \mathbb{R}^{B\times N}$) is the matrix form of intensity i, B is the mini-batch size and N is the number of capsules. Equation (5) requires the model to reconstruct an object by K capsules. Equation (6) requires each capsule can contribute $B \times K/N$ times in every mini batch. The final loss function is described as $L = L_{reg} + \alpha L_{s1} + \lambda L_{s2}$. Where α and λ are set to 1 and 0.1, respectively. (The value of α and λ is discussed in the Appendix.C.4).

4 Experiments

We implement our method based on the same setting. Details can be found in the Appendix.C.1. CAE is a vanilla capsule autoencoder without dynamic part representation. In subsection 4.2, we comprehensively evaluate the performance of our proposed DPR-CAE. In subsection 4.3, we implement an ablation study to prove the effectiveness of these components that make up the proposed method. In subsection 4.4, we extend our DPR-CAE to DPR-SCAE, and achieve state-of-the-art performance in unsupervised object classification. The code will be released.

4.1 Datasets

We evaluate our algorithm on the following, widely-used image datasets: **MNIST** [Lecun *et al.*, 1998] is a benchmark containing 70,000 hand-written digits. We use all images from the training set apart from their labels. **Fashion-MNIST** [Xiao *et al.*, 2017] consists of a training set of 60,000 examples and a test set of 10,000 examples. Each example from above both datasets is a 28×28 grayscale image. **SVHN** [Netzer *et al.*, 2011] and **CIFAR10** [Krizhevsky, 2009] consist of 32×32 colored images coming from 10 classes, which contain 99289 and 60,000 images, respectively. rm-X means applying random movement to the X dataset.

4.2 Main Resutls

Capsule autoencoder parses an image into part capsules, and then a learned template bank is regulated by these capsules to reconstruct output. Figure 1 reports the reconstruction error on four datasets. VAE [Kingma and Welling, 2014] is a baseline model (details in Appendix.C.2). The proposed DPR-CAE outperforms all its counterparts with a large margin on all datasets. CAE also outperforms the baseline on Fashion-MNIST, SVHN and CIFAR10 datasets. The results show that capsule autoencoder achieves lower error in reconstructing images by directly learning how to combine parts. Figure 5 visualizes the reconstruction results. It is obvious that the reconstructed image of VAE is smooth and losses a lot of details. Compared with VAE, the final image synthesized by CAE is composed of different local blocks. By introducing dynamic part representation, DPR-CAE achieves the best visualization effect in terms of overall and local details, especially in color images.

Figure 6 visualizes the difference of the intermediate process of the proposed CAE and DPR-CAE. Compared with traditional autoencoder methods, our models are more interpretable. It is easily observed that, compared to CAE (Figure 6 (a)), with introducing dynamic part representation, every part-object representations from the same capsule (each column in Figure 6 (b)) are rich and various. In addition, more complex parts are generated by the DPR-CAE, which is a fundamental improvement in its expressive ability. This phenomenon reflects the powerful expressiveness of dynamic part representation.

4.3 Ablation Study

We evaluate the effectiveness of components that make up the DPR-CAE. All models are trained with the same setting except one variable, 100 epochs are used in all ablation study. Table 1 reports which model components are important. The second and third rows show that no L_{s1} declines model performance, but that L_{s2} might not be necessary. Actually, without L_{s2} regularization, lots of part capsules are dead (Figure 7), which is undesirable for model's robustness. The

Figure 5: Visualization results from four datasets. For each part, the first row (blue box) indicates target images; the second row (green box) indicates VAE's reconstruction; the third row (yellow box) shows CAE's reconstruction; the last row (red box) shows DPR-CAE's reconstruction.

fourth and fifth row show that translation-invariant module and dynamic part representation are the key components to improve model performance. Without DPR, the reconstruction error sharply increases from 24.13 to 34.25 on CIFAR10 dataset. The last row reports the effectiveness without nonlinear activation introduced in section 3.2. No nonlinear activation increases the reconstruction error because all capsules trend to average value as visualized in Figure 7.

Table 2 investigates the impact of our models with different number of capsules. With increasing the number of capsules, the performance trends to be better until 20 capsules are used on SVHN and CIFAR10 datasets. Continuing to increase the number of capsules (25 capsules) may bring redundancy to this model, which could increase the burden of the models and thus reduce performance. The effectiveness of dimension of dynamic vector dy is discussed in Table 3. From the results it is obvious that the model's performance increases as the dimensionality increases, which is very reasonable. Higher dimensions can generate a richer representation for each part, thereby improving the overall performance of the model.

Methods	rm-SVHN	rm-CIFAR10
full model	16.92	24.13
no L_{s1}	17.54 (+0.62)	24.33 (+0.20)
no L_{s2}	**12.86 (-4.06)**	**18.52 (-5.61)**
no TIM	18.20 (+1.28)	32.21 (+8.08)
no DPR	19.13 (+2.21)	34.25 (+10.12)
no nonlinear activation	17.67 (+0.55)	25.11 (+0.98)

Table 1: Ablation study on SVHN and CIFAR10 datasets. Reconstruction errors are reported.

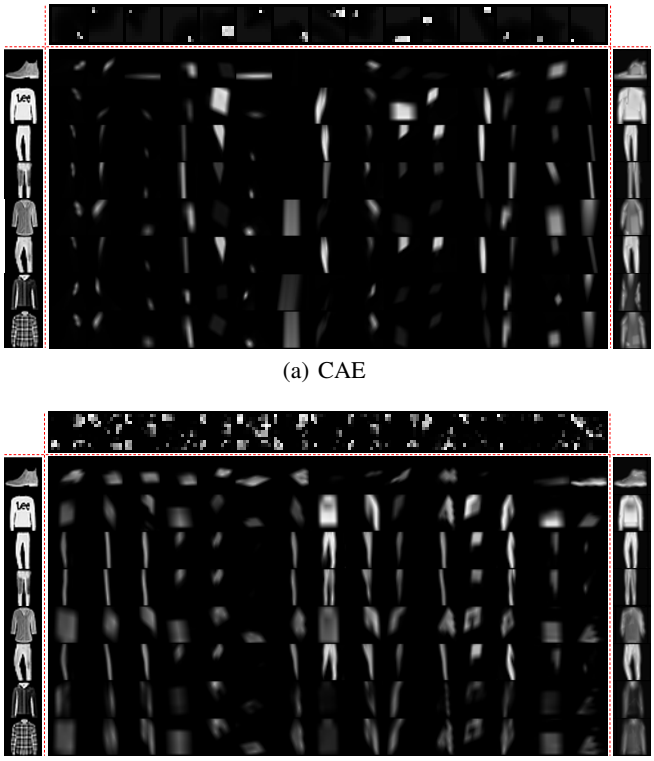

(a) CAE

(b) DPR-CAE

Figure 6: Visualize templates and part-object representations on Fashion-MNIST dataset. Top: template bank T; Left: input images; Mid: part-object representations $\hat{O}$; Right: composite images.

Capsules	SVHN	CIFAR10
10	18.46/18.88	36.91/28.86
15	17.37/13.18	34.63/27.40
20	**16.88**/12.51	**34.56/27.08**
25	18.56/**12.09**	36.04/28.61

Table 2: Reconstruction error with different number of capsules. '/' indicates 'CAE/DPR-CAE'.

4.4 Unsupervised Classification

Stack capsule autoencoder (SCAE) [Kosiorek *et al.*, 2019] is a powerful model in unsupervised classification. The template T is directly exploited in its PCAE module, which limits its latent ability. To further evaluate DPR-CAE, we replace the PCAE module with our DPR-CAE with some modifications (Appendix.C.3), called DPR-SCAE. For a fair comparison, we follow the same setting as used in SCAE.

Table 4 reports the unsupervised classification results com-

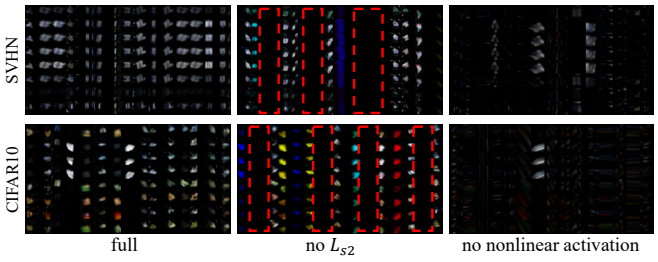

Figure 7: Visualization results of part-object representations. Dash red box indicates that, without no L_{s2} regularization, corresponding capsules are dead. Without no nonlinear activation, all capsules trend to average value so that the picture looks dark.

Dimensions	SVHN	CIFAR10
6	14.79	30.70
12	13.64	27.05
18	12.78	24.10
24	**12.69**	**24.05**

Table 3: Reconstruction error with different dimension of dynamic part representations.

pared with state-of-the-art methods. Our DPR-SCAE outperforms all its counterparts and achieves 97.98% and 72.56% accuracy on MNIST and Fashion-MNIST datasests, respectively. Especially on the Fashion-MNIST dataset, DPR-SCAE obtains a 12.02% absolute performance gain over its baseline SCAE, and surpasses second place VaGAN-SMM [Yang *et al.*, 2020] by 5.61% absolute accuracy.

To further demonstrate the robustness of the proposed translation-invariant module, we evaluate our DPR-SCAE with translation-invariant module on rm-MNIST and rm-Fashion-MNIST datasets. Table 5 reports that, with introducing random movement in the dataset, the performance of SCAE and DPR-SCAE is dramatically degraded. This phenomenon reflects that part capsules are troublesome to encode both object-part and scene-object relationships simultaneously. With introducing translation-invariant module, the scene-object relationship is encoded by our translation-invariant module, and the DPR-CAE only needs to focus on

Methods	MNIST	F-MNIST
DEC [Xie *et al.*, 2016]	84.03	59.48
IDEC [Guo *et al.*, 2017]	88.06	60.88
DAG [Harchaoui *et al.*, 2017]	94.08	-
GMVAE [Dilokthanakul *et al.*, 2017]	86.01	59.56
VaDE [Jiang *et al.*, 2017]	94.46	62.87
InfoGAN [Chen *et al.*, 2016]	89.00	61.00
ClusterGAN [Mukherjee *et al.*, 2019]	95.00	63.00
VaGAN-SMM [Yang *et al.*, 2020]	95.75	66.95
DANDSC [Yang *et al.*, 2019]	97.80	66.20
SCAE* [Kosiorek *et al.*, 2019]	96.75	60.54
DPR-SCAE (ours)	**97.98**	**72.56**

Table 4: Unsupervised classification on MNIST and Fashion-MNIST datasets. '*' indicates the reported results from the reimplemented code by ourselves.

Methods	rm-MNIST	rm-F-MNIST
SCAE	81.33	48.86
SCAE†	95.17 (+**13.84**)	54.88 (+**6.02**)
DPR-SCAE	84.61	48.85
DPR-SCAE†	93.99 (+**9.38**)	68.05 (+**19.20**)

Table 5: Robust results of our proposed translation-invariant module. † indicates using translation-invariant module. 'rm-' means objects are random movement in the scene.

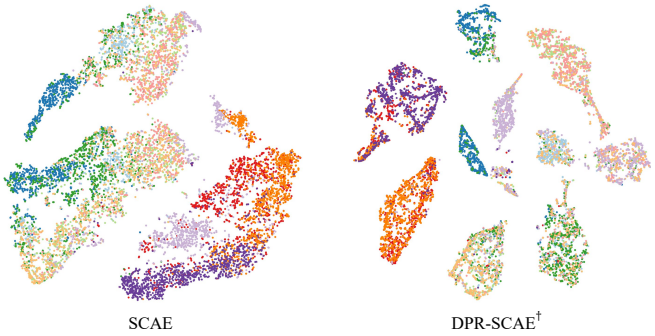

Figure 8: Comparison TSNE embeddings of object capsule presence probabilities for 10000 rm-Fashion-MNIST images.

encoding object-part relationship, which leads to an evident performance improvement. SCAE with translation-invariant module achieves 13.84% and 6.02% absolute accuracy improvement on rm-MNIST and rm-F-MNIST datasets, respectively. DPR-SCAE with translation-invariant module achieves 9.38% and 19.20% absolute accuracy improvement on rm-MNIST and rm-F-MNIST datasets, repectively. Figure 8 compares the TSNE embeddings of object capsule presence probabilities for rm-Fashion-MNIST val set between SCAE and DPR-SACE†. Obviously, DPR-SCAE† can better distinguish different types of features effectively. More visualization results can be found in Appendix.C.5.

5 Conclusions

In this paper, we provide an unsupervised capsule network framework to parse an image into interpretable parts, called DPR-CAE. The part representations in our method are dynamically generated by combining the dynamic vector and a shared template bank, which endows our model a powerful capability for representing complex samples. A translation-invariant module is introduced to avoid directly encoding the uncertain scene-part relationship in our DPR-CAE, which improves the model's robustness. Furthermore, we extend DPR-CAE into stacked capsule autoencoder by replacing PCAE with the DPR-CAE, namely DPR-SCAE. Despite being trained in an unsupervised fashion, our representation achieves state-of-the-art performance across reconstruction, classification. DPR-CAE can effectively obtain the part representations for an image, while it can't be a generator due to unknown latent space. Thus, to further develop a capsule variational autoencoder based on the DPR-CAE is the next work. We argue that it can serve as a strong baseline to generate interpretable high-quality images.

References

[Chen *et al.*, 2016] X. Chen, Y. Duan, R. Houthooft, J. Schulman, I. Sutskever, and P. Abbeel. Infogan: Interpretable representation learning by information maximizing generative adversarial nets. In *Advances in Neural Information Processing Systems (NeurIPS)*, page 2180–2188, 2016.

[Dilokthanakul *et al.*, 2017] N. Dilokthanakul, P. A. M. Mediano, M. Garnelo, Matthew C. H. Lee, H. Salimbeni, K. Arulkumaran, and M. Shanahan. Deep unsupervised clustering with gaussian mixture variational autoencoders, 2017.

[Duarte *et al.*, 2019] K. Duarte, Y. Rawat, and M. Shah. Capsulevos: Semi-supervised video object segmentation using capsule routing. In *International Conference on Computer Vision (ICCV)*, pages 8479–8488, 2019.

[Edraki *et al.*, 2020] M. Edraki, N. Rahnavard, and M. Shah. Subspace capsule network. In *Association for the Advancement of Artificial Intelligence (AAAI)*, pages 10745–10753, 2020.

[Guo *et al.*, 2017] X. Guo, L. Gao, X. Liu, and J. Yin. Improved deep embedded clustering with local structure preservation. In *International Joint Conferences on Artificial Intelligence (IJCAI)*, pages 1753–1759, 2017.

[Harchaoui *et al.*, 2017] W. Harchaoui, P. Mattei, and C. Bouveyron. Deep adversarial gaussian mixture autoencoder for clustering, 2017.

[Hinton *et al.*, 2011] G. E. Hinton, A. Krizhevsky, and S. Wang. Transforming auto-encoders. In *International Conference on Artificial Neural Networks (ICANN)*, pages 44–51, 2011.

[Hinton *et al.*, 2018] G. E Hinton, S. Sabour, and N. Frosst. Matrix capsules with EM routing. In *International Conference on Learning Representations (ICLR)*, 2018.

[Jaderberg *et al.*, 2015] M. Jaderberg, K. Simonyan, A. Zisserman, and K. Kavukcuoglu. Spatial transformer networks. In *Advances in Neural Information Processing Systems (NeurIPS)*, 2015.

[Jiang *et al.*, 2017] Z. Jiang, Y. Zheng, H. Tan, B. Tang, and H. Zhou. Variational deep embedding: An unsupervised and generative approach to clustering. In *International Joint Conferences on Artificial Intelligence (IJCAI)*, page 1965–1972, 2017.

[Kingma and Welling, 2014] D. P Kingma and M. Welling. Auto-encoding variational bayes. In *International Conference on Learning Representations (ICLR)*, 2014.

[Kosiorek *et al.*, 2019] A. R. Kosiorek, S. Sabour, Y. Teh, and G. E. Hinton. Stacked capsule autoencoders. In *Advances in Neural Information Processing Systems (NeurIPS)*, 2019.

[Krizhevsky, 2009] A. Krizhevsky. Learning multiple layers of features from tiny images. 2009.

[Lecun *et al.*, 1998] Y. Lecun, L. Bottou, Y. Bengio, and P. Haffner. Gradient-based learning applied to document recognition. *Proceedings of the IEEE*, 86(11):2278–2324, 1998.

[Mukherjee *et al.*, 2019] S. Mukherjee, H. Asnani, E. Lin, and S. Kannan. Clustergan : Latent space clustering in generative adversarial networks, 2019.

[Netzer *et al.*, 2011] Y. Netzer, T. Wang, A. Coates, A. Bissacco, B. Wu, and A. Ng. Reading digits in natural images with unsupervised feature learning. 2011.

[Ribeiro *et al.*, 2020a] D. S. Ribeiro, Fabio, Leontidis, Georgios, Kollias, and Stefanos. Capsule routing via variational bayes. In *Association for the Advancement of Artificial Intelligence (AAAI)*, volume 34, pages 3749–3756, Apr. 2020.

[Ribeiro *et al.*, 2020b] F. Ribeiro, G. Leontidis, and S. Kollias. Introducing routing uncertainty in capsule networks. In *Advances in Neural Information Processing Systems (NeurIPS)*, 2020.

[Sabour *et al.*, 2017] S. Sabour, N. Frosst, and G. E Hinton. Dynamic routing between capsules. In *Advances in Neural Information Processing Systems (NeurIPS)*, 2017.

[Taeyoung *et al.*, 2019] H. Taeyoung, P. Myeongjang, and K. Gunhee. Self-routing capsule networks. In *Advances in Neural Information Processing Systems (NeurIPS)*, volume 32, pages 7658–7667, 2019.

[Tieleman, 2014] T. Tieleman. Optimizing neural networks that generate images, 2014.

[Wang and Liu, 2018] D. Wang and Q. Liu. An optimization view on dynamic routing between capsules. In *International Conference on Learning Representations*, 2018.

[Xiang *et al.*, 2018] C. Xiang, L. Zhang, Y. Tang, W. Zou, and C. Xu. Ms-capsnet: A novel multi-scale capsule network. *IEEE Signal Processing Letters*, 25(12):1850–1854, 2018.

[Xiang *et al.*, 2020] C. Xiang, Z. Wang, S. Tian, J. Liao, W. Zou, and C. Xu. Matrix capsule convolutional projection for deep feature learning. *IEEE Signal Processing Letters*, 27:1899–1903, 2020.

[Xiao *et al.*, 2017] H. Xiao, K. Rasul, and R. Vollgraf. Fashion-mnist: a novel image dataset for benchmarking machine learning algorithms, 2017.

[Xie *et al.*, 2016] J. Xie, R. Girshick, and A. Farhadi. Unsupervised deep embedding for clustering analysis, 2016.

[Yang *et al.*, 2019] X. Yang, C. Deng, F. Zheng, J. Yan, and W. Liu. Deep spectral clustering using dual autoencoder network. In *Conference on Computer Vision and Pattern Recognition (CVPR)*, pages 4061–4070, 2019.

[Yang *et al.*, 2020] L. Yang, W. Fan, and N. Bouguila. Clustering analysis via deep generative models with mixture models. *IEEE Transactions on Neural Networks and Learning Systems*, pages 1–11, 2020.

[Zhang *et al.*, 2018] L. Zhang, M. Edraki, and G. Qi. Cappronet: Deep feature learning via orthogonal projections onto capsule subspaces. In *Advances in Neural Information Processing Systems (NeurIPS)*, 2018.

Layers	channels	kernels	strides
1	128	3	2
2	128	3	2
3	128	3	1
4	128	3	1
5	$(N * (6 + 1 + A + 1))$	1	1

Table 6: Architecture details.

A Part encoder architecture

The part encoder consists of a CNN followed by a bottom-up attention mechanism based on global-average pooling, details in Table 6. The CNN contains four layers with 128 channels. All kernels are 3×3, and first two layers with a stride of two. We use Relu nonlinearities for all layers. The fifth layer is the attention-based pooling. Its input channel is set to 128, and output channel is set to $(N \times (6 + 1 + A + 1))$. N is the number of capsules. For every part capsule n, we use the CNN to predict a feature map c_n of 6(pose) + 1(intensity)+A(dy) capsule parameters, as well as a single-channel attention mask a_n. We implement the attention mechanism as [Kosiorek *et al.*, 2019].

B Translation-invariant module

In our experiments, we plug translation-invariant module into the CNN encoder to translate image feature into a standard feature space. The prediction network is a simple CNN. The first layer is a convolutional layer with 3×3 kernels and 2 strides. The second layer is a full connection layer with 128 units. The final layer is a full connection layer with 4 outputs. Suppose the final outputs are $[sx, sy, x, y]$, we define the parameter θ as follows:

$$\theta = \begin{bmatrix} sx & 0 & x \\ 0 & sy & y \\ 0 & 0 & 1 \end{bmatrix} \tag{7}$$

and its inverse define as:

$$\theta^{-1} = \begin{bmatrix} \frac{1}{sx} & 0 & -\frac{x}{sx} \\ 0 & \frac{1}{sy} & -\frac{y}{sy} \\ 0 & 0 & 1 \end{bmatrix} \tag{8}$$

The transformation processing follows [Jaderberg *et al.*, 2015]. The θ translates the object in the scene into a standard coordinate frame, and θ^{-1} translates the composite object into the scene.

C Supplementary experiments

C.1 Training details

All models are trained with the RMSProp optimizer ($momentum = 0.9$ and $\epsilon = (10 * batch\_size)^{-2}$). Batch size is set to 64 for MNIST and Fashion-MNIST 256 for SVHN and CIFAR10 datasets. The learning rate was equal to 3×10^{-5} for all datasets and exponential learning rate decay of 0.997 every 10^3 weight updates. 1000 epochs are used in main experiments, and 100 epochs are used in ablation study. For DPR-SCAE, we follows the same setting used in [Kosiorek *et al.*, 2019].

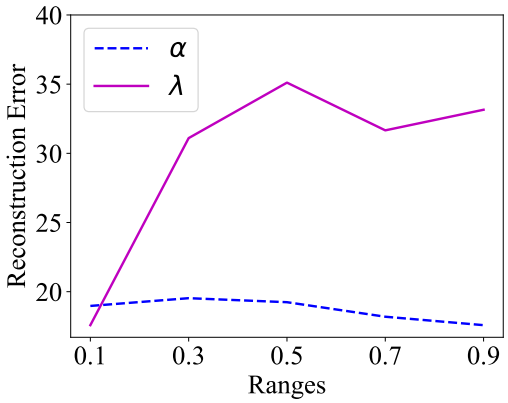

Figure 9: The reconstruction error on rm-SVHN dataset.

C.2 VAE baseline

VAE consists of the encoder and decoder. The encoder is a full connection network with 3 layers. The input layer contains $H \times W \times C$ units. Where H, W, and C indicates the high, width, and channel of the input image, respectively. The hidden layer contains 128 units. The code layer contains 20 and 40 units (mean and variance) for grayscale and colored images respectively. Relu activation function is used in the first two layers. The decode contains 3 layer full connection layers. The number of units is set to 10 and 20 for grayscale and colored images respectively. The hidden layer contains 128 units. The output layer contains $H \times W \times C$ units. Relu activation function is used in the first two layers, and the Sigmoid activation function is used in the output layer. The prior distribution is a standard Gaussian distribution for all datasets.

C.3 DPR-SCAE architecture

We replace PCAE in SCAE with our DPR-CAE with some modifications. 1) The dynamic vector is generated by a simple MLP with 3 layers, in which the input is the special features z. 2) We calculate the image likelihood used in SCAE rather than reconstruction error to optimizer the model.

C.4 The value of α and λ

We discuss the value range of α and λ, as shown in Figure 9. The results show that increasing the λ sharply leads to a big reconstruction error. Considering to the model's diversity as discussed in Section 4.3, we set λ to 0.1 in practice. In contrast, α has an inverse trending for reconstruction error, and we set it to 1 in practice.

C.5 More visualization results

Some of visualization results of DPR-SCAE are shown in Figure 10 and Figure 11.

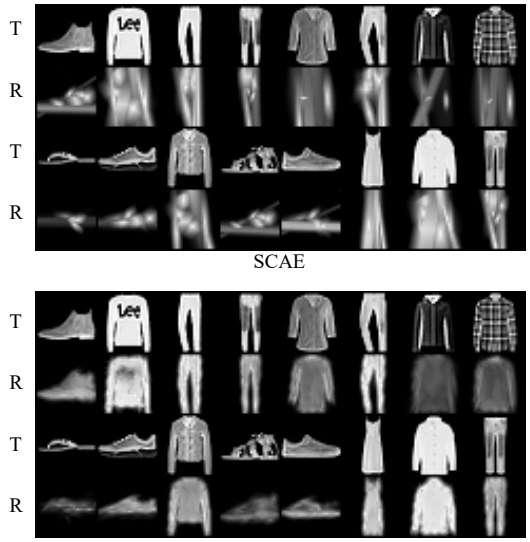

Figure 10: Comparison visualization results of SCAE and DPR-SCAE on Fashion-MNIST dataset. 'T' means target image, 'R' means reconstruction images

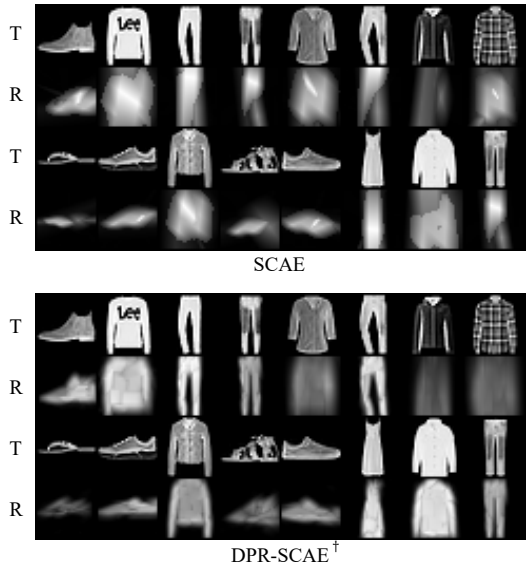

Figure 11: Comparison visualization results of SCAE and DPR-SCAE† on rm-Fashion-MNIST dataset. 'T' means target image, 'R' means reconstruction images